Experimental Analysis of Millimeter Wave Coplanar Waveguide Slow Wave Structures on GaAs

Ralph Spickermann and Nadir Dagli, *Member, IEEE*

Abstract— **Microwave coplanar waveguide slow wave structures suitable for use in traveling wave electrooptic modulators were experimentally investigated to 40 GHz. Velocity slowing is achieved by introducing periodic slots in the ground planes. Structures both on semiinsulating GaAs substrates and on epitaxial layers grown by molecular beam epitaxy on semi-insulating GaAs substrates were examined. In the measurements the thru-reflect-line calibration method was used and its limitations are discussed. The characteristic impedance, phase velocity and loss coefficient of these lines were extracted from measured S-parameters. Effects of various dimensions on these line properties are presented and discussed. Results indicate that significant phase velocity slowing without dispersion at least up to 40 GHz is possible with this approach. This is true both on semi-insulating GaAs substrates and specially designed epitaxial layers. A design approach to achieve a specified phase velocity and characteristic impedance is given.**

I. Introduction

MONOLITHIC microwave transmission lines such as microstrip and coplanar lines are the basic components of monolithic high frequency circuits. They need to be specially designed for applications where a specific value of the phase velocity over a wide frequency range is necessary. A few examples of such applications are compact delay lines, phase shifters and traveling-wave electrooptic modulators. The authors are mainly concerned with traveling-wave electrooptic modulators that offer very wide electrical bandwidths [1]. Although the electrode geometry studied in this work is suitable for a modulator application, the actual modulator design is beyond the scope of this paper and will be discussed in another publication. As discussed in [1], the largest bandwidths in traveling wave electrooptic modulators are achieved by matching the phase velocities of the microwave and optical signals. In III-V compound semiconductors this necessitates the slowing of the microwave signal [2], [3]. This paper investigates a type of monolithic microwave coplanar transmission line that can achieve a desired amount of phase velocity reduction and a desired characteristic impedance value simultaneously.

Such lines are realized using periodically loaded slow wave structures. These have been investigated by different groups [2], [4]–[7]. A recent paper studied a slow wave structure based on a two conductor coplanar strip waveguide [7]. In our work a three conductor coplanar transmission line is chosen because of its planar structure and suitability to a push pull Mach-Zehnder electrooptic modulator electrode design. The goal is defined to realize a coplanar waveguide on GaAs with a 50 Ω characteristic impedance and a phase velocity of 8.9 cm/nsec, which is about the phase velocity of an optical signal in GaAs with a free space wavelength of 1.3 μm. This phase velocity goal requires a reduction of approximately 22% from that of a smooth coplanar line on this material. The approach described and the results presented may be applicable to other situations where a prescribed velocity reduction coupled with a specific line characteristic impedance is desired.

Manuscript received December 17, 1992; revised December 7, 1993. This work is supported in part by a UC MICRO/Tektronix grant and in part by ARPA grants MDA972–94–1–0002 and DABT63–93–C-0039.

The authors are with the Department of Electrical and Computer Engineering, University of California, Santa Barbara, CA 93106 USA.

IEEE Log Number 9404141.

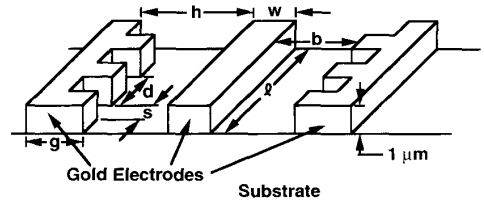

Fig. 1. Schematic of the coplanar slow wave structures discussed in this work. Substrate is either semi-insulating GaAs or MBE grown unintentionally doped epitaxial layers on semi-insulating GaAs. Superstrate is air.

The approach taken in this paper is mainly experimental. This involved the fabrication and characterization of two hundred and fourteen lines of different dimensions up to 40 GHz. The range of line parameters that needed to be covered was determined using approximate models.

The organization of this paper is as follows: In Section II the basic slow wave structure used in this work and the selection of the range of the parameters involved are described. Section III covers the fabrication and inspection of devices. In Section IV the measurement method used and the issues involved in the extraction of parameters are discussed. In Section V the experimental results are given and the method of selecting a design for a particular phase velocity and characteristic impedance is outlined. In Section VI, the performance on an unintentionally doped molecular beam epitaxy (MBE) grown optical guide structure similar to that to be used for the modulator is investigated. Finally, conclusions of this work are given.

II. Coplanar Waveguide Slow Wave Structure

Fig. 1 schematically illustrates the slow wave lines studied in this work. They are modified coplanar microwave lines either on semi-insulating GaAs substrates or MBE grown unintentionally doped epitaxial layers on semi-insulating GaAs substrates. As shown in Fig. 1, periodic slots are cut into the ground electrodes. The periodic slots result in a slower phase

velocity compared to the smooth geometry [6]. The labeling shown in this figure for various mechanical dimensions will be used in the rest of this paper. This paper describes the tailoring of these dimensions to achieve a desired characteristic impedance and phase velocity.

There are any number of geometries which can achieve velocity slowing. The one chosen in this work was selected because of its simplicity and ease of fabrication as well as its suitability for the modulator as a whole. A small periodicity $d = 50\ \mu$m was chosen to stay well away from the cutoff frequency of the structure so that dispersion is minimized [6]. The cutoff frequency at the phase velocity goal for $d = 50\ \mu$m is approximately

$$f_{\text{cutoff}} \cong \frac{v_{\text{ph}}}{2d} = \frac{8.9\ \text{cm/n sec}}{2 \cdot 50\ \mu\text{m}} = 890\ \text{GHz}. \qquad (1)$$

This indicates that for frequencies below 100 GHz dispersion due to the periodicity of the structure is negligible. A small cross sectional geometry is necessary to match the small size of the optical guides with which it is to be integrated.

Once the basic structure and limitations on its periodicity and cross sectional geometry were determined, the range of the other parameters shown in Fig. 1 was investigated. The accurate modeling of this structure is a complicated problem. Rather than doing this, several different simple equivalent circuit approaches were used. The goal of modeling was to roughly indicate if these structures could sufficiently reduce the phase velocity and if so what ranges of parameters would be required. Each of these models was based on a different equivalent circuit for one period (a "unit cell") of the line [8]. The inductance and capacitance per unit length (L and C) of the ideal line sections contained in these unit cell models were calculated using a two dimensional finite element simulator [9]. The ABCD matrix of the cell was then calculated using transmission line theory. From this ABCD matrix any conceivable property of the line may be extracted [8].

The modeling predicted that the required slowing could be achieved, and indicated a set of dimensions to meet the performance specifications outlined in the introduction. These dimensions were $b = 9\ \mu$m, $d = 50\ \mu$m, $h = 30\ \mu$m, $s = 15\ \mu$m, and $w = 20\ \mu$m. Dimension g which determines the width of the ground plane was chosen to be 206 μm through use of the finite element simulator [9]. For g values larger than this, L and C vary less than 1% as the ground plane width varies. A nominal line length of $l = 1$ cm was chosen, which is on the order of the length necessary for the modulator application.

Different combinations of b, h, l, and w values around the values indicated above were chosen. For each combination, the s/d ratio was varied from 0 to 1. Note that s/d values of 0 and 1 correspond to uniform coplanar lines. The range of parameters were $l = 1$, 2, or 3 cm, $5\ \mu\text{m} < b < 15\ \mu$m, $20\ \mu\text{m} < h < 80\ \mu$m, $15\ \mu\text{m} < w < 35\ \mu$m.

Two hundred and fourteen different lines with integrated microwave probe pad structures were laid out. The pad structures were designed to mate with 150 μm pitch ground-signal-ground probes. A typical line geometry with pads is shown in Fig. 2(a).

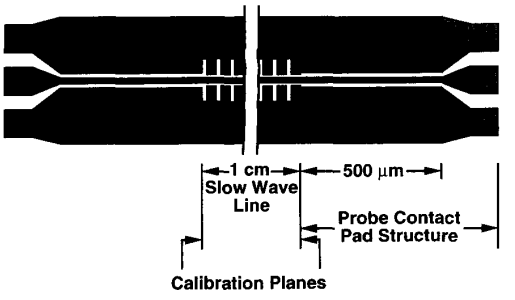

(a)

(b)

Fig. 2. (a) To scale schematic of the entire fabricated (9,65,20) $s/d = 0.3$ line with $b = 9\ \mu$m, $h = 65\ \mu$m and $w = 20\ \mu$m. (b) Photo showing the transition from the contact pad structure to the slow wave structure. The dark spots in the gold are gold lumps caused by the electron beam evaporator used to deposit the gold.

III. Fabrication and Mechanical Inspection

The lines were fabricated using a lift-off technique on 2″ diameter 670 μm thick semi-insulating GaAs wafers. The metal was deposited using an electron beam evaporator. It consisted of 100 Å of Ti, 100 Å of Pt and $\sim 10,000$ Å of Au. After fabrication each wafer was carefully inspected. The total metal thickness was measured at four different places per wafer using a DekTak surface profiler, and was found to be uniform at ~ 9500 Å. Each line was then inspected visually with a microscope along its entire length. A 93% yield was observed. A photograph of a unit cell in each line was taken to measure the final electrode dimensions. The widths of the fabricated lines were generally about 0 to 0.3 μm larger than the designed values which is a negligible variation. Hence for all practical purposes the line cross sectional dimensions are identical to the design values. Fig. 2(b) is a photograph of a typical fabricated line.

IV. Measurement Technique

S-parameters of the lines were measured from 2 to 40 GHz at 101 equally spaced frequencies with an HP8510B Automatic Network Analyzer. The lines were probed on-wafer using a Cascade Microtech Probe Station with Tektronix 150 μm pitch ground-signal-ground probes. The signals were transmitted between the network analyzer and the probes with Wiltron K-120 semi-rigid cables.

For calibration purposes the through-reflect-line ("trl") calibration method detailed in reference [10] was used. The

calibration standards in this method are a user constructed set of through lines and shorts. A characteristic impedance value of 50 Ω was chosen for the through lines. The calibration set was designed using the finite element simulator [9]. Because the entire calibration relies on the assumption that the through lines in the calibration standards have 50 Ω impedance, their design was triple checked using another recently developed tool [11] as well as with the commercial program "linecalc" [12]. These three methods all showed agreement to within 1 Ω. Nine of these calibration sets were placed between the groups of slow wave structures on each mask, and were fabricated along with the devices on the same wafer.

This calibration scheme allows one to bring the reference planes to the end points of the slow wave structures as shown in Fig. 2(a). Therefore, probe tip to pad structure transition effects which may become important around 40 GHz are calibrated out. However, it is important to realize the intrinsic limitations of the trl calibration method used in this work. All of the computer software used to design the 50 Ω through lines assume waveguides made of perfect conductors on ideal dielectrics. Hence, the "internal inductance" contribution to L due to field penetration into the conductors is not accounted for. At the higher frequencies of the measurement band this is acceptable because the skin depth and hence field penetration is minimal. Additionally, at high frequencies the frequency dependent terms will dominate the ohmic loss terms R and G in the characteristic impedance expression which is

$$Z_0 = \sqrt{\frac{R + j\omega L}{G + j\omega C}} \tag{2}$$

where R and G are the resistance and conductance per unit length of the transmission line. Note that R increases with frequency due to skin depth effects. However typical values for the lines used in this work are $\omega C/G > 1000$ and $\omega L/R \sim 25$ at 35 GHz. Therefore R and G can be neglected meaning that the perfect conductor and ideal dielectric approximations hold. One can see that if the line cross sections were any smaller, R would increase further, and the perfect conductor assumption might lose its validity. In order to use this calibration method, these ratios must be confirmed to be large for the structure and frequencies under consideration. This can be done by calculating DC resistance of the lines and using the values of L and C given by whatever perfect conductor modeling tool is being used to design the calibration standards.

However at lower frequencies, for example at 3 GHz, this calibration technique can lead to serious error for lines of this small cross sectional profile. Here the real lossy terms are no longer negligible compared to the frequency dependent terms and the characteristic impedance is no longer purely real, but approaches

$$Z_0 \cong \frac{1-j}{\sqrt{2}}\sqrt{\frac{R}{\omega C}} \tag{3}$$

as R becomes much larger than ωL [13]. Then the 50 Ω real impedance definition given to the through lines as the basis of the calibration is no longer valid. For the structures studied in this work, at 3 GHz $\omega L/R \approx 2$, so the calibration is beginning to break down.

This argument shows that at higher frequencies the perfect conductor assumption and the accuracy of the calibration are very good. For modulator applications the values of v_{ph} at higher frequencies are of principal interest, because below 5 GHz the wavelengths are long relative to typical device length and the phase velocity mismatch is not a problem [1]. Therefore the trl calibration scheme with user defined standards on the same substrate as the devices being measured is appropriate for characterization of these structures for this application.

Once the S-parameters are measured the line parameters are obtained by calculating the ABCD matrix representing the entire transmission line in between the reference planes. Note that this is not the ABCD matrix of the unit cell of the line utilized earlier in modeling. The ABCD matrix depends on the measured S-parameters as follows [13]:

$$\begin{bmatrix} A & B \\ C & D \end{bmatrix} = \begin{bmatrix} \frac{(1+s_{11})(1-s_{22})+s_{12}s_{21}}{2s_{21}} & Z_{0R}\frac{(1+s_{11})(1+s_{22})-s_{12}s_{21}}{2s_{21}} \\ \frac{1}{Z_{0R}}\frac{(1-s_{11})(1-s_{22})-s_{12}s_{21}}{2s_{21}} & \frac{(1-s_{11})(1+s_{22})+s_{12}s_{21}}{2s_{21}} \end{bmatrix}. \tag{4}$$

Here Z_{0R} is the impedance reference, which in our case is 50 Ω. The complex characteristic impedance Z_0 and complex propagation constant γ of the line can then be found [8]:

$$Z_0 = \frac{2B}{D - A \pm \sqrt{(A+D)^2 - 4}} \tag{5}$$

$$\gamma = \frac{1}{l}\left[\ln\left(\left(\frac{A+D}{2}\right) \pm \sqrt{\left(\frac{A+D}{2}\right)^2 - 1}\right)\right]. \tag{6}$$

Here, l is the length of the transmission line. The propagation constant γ may be decomposed as $\gamma = \alpha + j\beta$, where α is the attenuation coefficient (Np/unit length) and β is the phase constant (rad/unit length). Note that (5) and (6) are doubled valued. The physically meaningful value of Z_0 is positive. The physically meaningful value of γ has a positive α. The phase velocity v_{ph} is then found as

$$v_{\mathrm{ph}} = \frac{2\pi f}{\beta}. \tag{7}$$

As mentioned above, the high frequency data is of the most importance. Throughout this work, if no frequency dependence is indicated the quoted values are measured at 35 GHz. These 35 GHz values were arrived at as follows. First, the data in the vicinity of frequencies where the line becomes resonant was discarded. This is because at those frequencies s_{11} and s_{22} approach zero and their accurate determination is no longer possible. Then a seven term least squares fit model was applied to the remaining points from which a value at 35 GHz was calculated along with a standard deviation error bar.

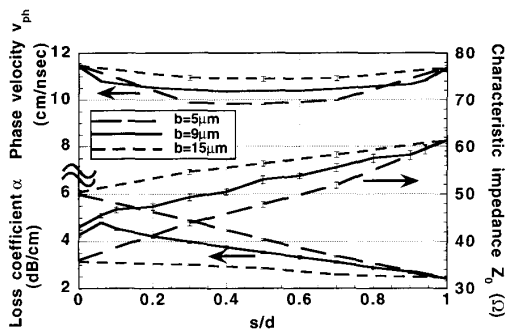

Fig. 3. Variation of $v_{\rm ph}$, Z_0 and α with gap width b for $h = 30$ μm, and $w = 20$ μm.

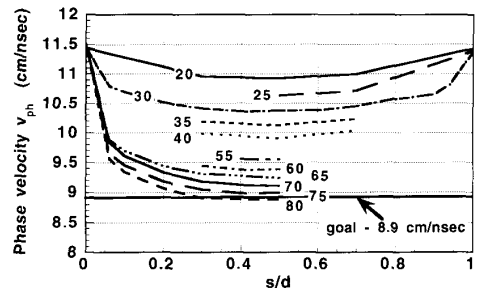

Fig. 4. Behavior of $v_{\rm ph}$ as a function of s/d with h as a parameter for $b = 9$ μm, $w = 20$ μm. The values of h (in μm) are indicated on the curves. Gaps in the $s/d < 0.5$ range of the curves are either due to missing data because of finite yield or for clarity. For $h > 40$ μm the $s/d > 0.5$ lines were not fabricated. In reality all the curves converge at $s/d = 0$ and $s/d = 1$.

V. Results On Lines Fabricated on Semi-Insulating GaAs Substrates

In this section the measurement results are given by describing the effects of changing b, h and w on $v_{\rm ph}$, Z_0, and α. These three measured line characteristics did not change at all for line length variation of 1, 2, and 3 cm which verifies the accuracy of the measurement and analysis method. Lines are labeled as (b, h, w), where b, h, and w are the parameters defined in Fig. 1 with units of μm. For example (5, 30, 20) is a line for which $b = 5$ μm, $h = 30$ μm, and $w = 20$ μm. Other values are kept constant at $d = 50$ μm, $g = 206$ μm, and $l = 1$ cm. In the figures data points are connected by straight lines. In many of the figures, the regions of $0 < s/d < 0.3$ and $0.7 < s/d < 1.0$ were explored in detail only for one particular b, h, and w combination. Therefore, plotted results for other b, h, and w combinations crossed over the results for the particular line investigated in detail due to the lack of data points in these regions, i.e., when data points $s/d = 0$, 0.3, or $s/d = 0.7$, 1.0 are connected by a straight line. This happened primarily in the $v_{\rm ph}$ graphs. In reality, all the plots have the same qualitative shape and do not cross.

The result of varying the gap width b is shown in Fig. 3. One can see that for narrow gaps the slots have a greater effect on $v_{\rm ph}$. For smaller gaps the field strength in the gaps is larger hence associated modes are perturbed more by the slots. At $s/d = 0$ the $v_{\rm ph}$ values coincide well, indicating that changing the gap on the smooth lines had little effect on $v_{\rm ph}$ as expected [14]. For $s/d = 1$ all the lines become identical, hence the results become identical at this point. The "bathtub" shape of the $v_{\rm ph}$ graph indicates that nearly all of the $v_{\rm ph}$ change possible for a given h is obtainable with $s/d \cong 0.3$. Fig. 3 also shows that Z_0 decreases as the gap gets smaller as expected. Z_0 changes almost linearly as a function of s/d for this value of h. Therefore, for small values of h (< 40 μm) Z_0 may be calculated by taking the weighted average of the impedances of the $s/d = 0$ and $s/d = 1$ lines according to their fractions in the unit cell. Fig. 3 also shows the variation of α as a function of s/d for different b values. As expected, α increases as b gets smaller indicating greater field concentration and current crowding for narrower gaps.

One might expect that an increase in h would cause an increase in α due to an increase in R resulting from longer current paths around the slots in the ground planes. While R is certainly increasing, Z_0 also increases and α which can be estimated as

$$\alpha \approx \frac{R}{2Z_0} \tag{8}$$

does not increase in direct proportion to R. This result shows that one can achieve $v_{\rm ph}$ reduction without being penalized with increased α due to the presence of slots. In fact, little variation in α with h up to 80 μm was observed.

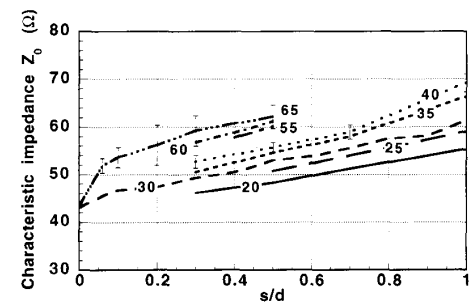

Fig. 5. Behavior of Z_0 as a function of s/d with h as a parameter for $b = 9$ μm, $w = 20$ μm. The values of h (in μm) are indicated on the curves. Gaps in the $s/d < 0.5$ range of the curves are either due to missing data because of yield or for clarity. For $h > 40$ μm the $s/d > 0.5$ lines were not fabricated. In reality all the curves converge at $s/d = 0$ and $s/d = 1$.

Fig. 4 shows the $v_{\rm ph}$ variation as a function of s/d for a wide range of h. The measured $v_{\rm ph}$ variation is roughly symmetric with respect to s/d up to $h = 40$ μm and it is assumed that this symmetry holds for larger h values. For $h > 40$ μm only the range up to $s/d = 0.5$ was investigated. The $v_{\rm ph}$ goal was reached with $h = 80$ μm at $s/d = 0.35$. Fig. 5 shows the variation of Z_0 for different h values. The data for $h > 65$ μm are not shown because for this range the accurate extraction of Z_0 becomes difficult. This is due to the mode mismatch reflection at the pad structure/slow wave line interfaces. These interfaces are at the calibration planes shown in Fig. 2(a). For large h values this reflection becomes larger than the reflection caused by the impedance mismatch. This mode mismatch reflection is not accounted for in the calibration and results in a distortion of the extracted

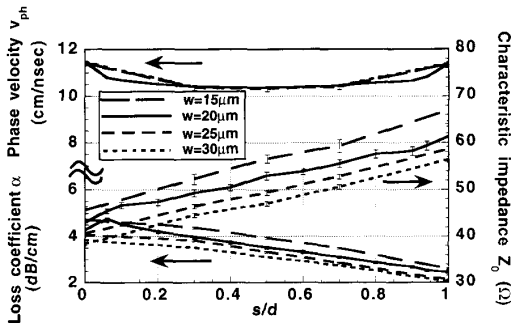

Fig. 6. Variation of $v_{\rm ph}$, Z_0 and α with center conductor width w for $b = 9$ μm, $h = 30$ μm. Note that only $w = 20$ μm was explored for $0 < s/d < 0.3$ and $0.7 < s/d < 1.0$. Data points in these regions are missing in the other graphs, and that is why a cross over appears. In reality the $v_{\rm ph}$ graphs all coincide.

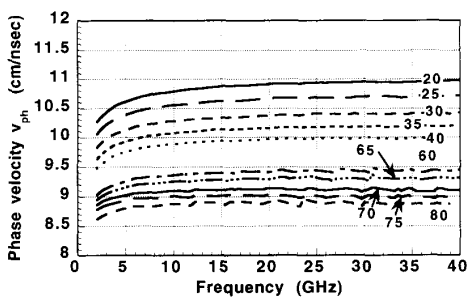

Fig. 7. Behavior of $v_{\rm ph}$ as a function of frequency at $s/d = 0.3$ with h as a parameter for $b = 9$ μm, $w = 20$ μm. The values of h (in μm) are indicated on the curves.

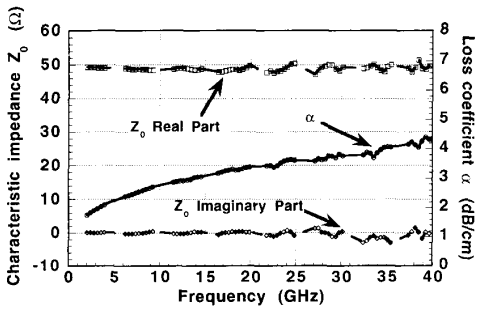

Fig. 8. Behavior of Z_0 and α as a function of frequency at $s/d = 0.3$ for the (9,30,20) line.

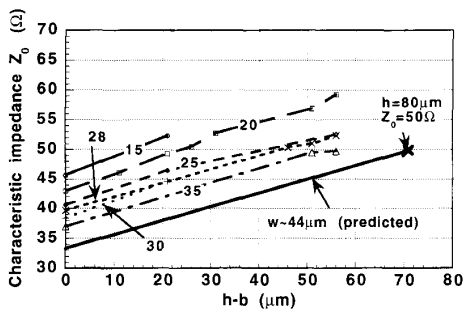

Fig. 9. Map of Z_0 as a function of slot depth $h - b$ with w as a parameter at $s/d = 0.3$ with $b = 9$ μm. The values of w (in μm) are indicated on the curves. The solid line is the result of extrapolation to reach the design goal of $v_{\rm ph} = 8.9$ cm/nsec with $Z_0 = 50$ Ω.

impedance value. This problem is expected to affect all the extracted line parameter values but it shows up first in the Z_0 results. This is because of the three line characteristics being studied, Z_0 is the most sensitive to the reflection S-parameters s_{11} and s_{22}, and s_{11} and s_{22} are the measurement parameters that are most severely affected by the mode mismatch.

Fig. 6 illustrates the effect of changing the center conductor width w. It shows the most striking property of these lines: changing the center conductor width has no effect on $v_{\rm ph}$ for any s/d. However, as also shown in Fig. 6, changing w does change Z_0. This allows setting $v_{\rm ph}$ by appropriately choosing b and h and then adjusting Z_0 independently with w. As described later, this was in fact what was done to arrive at the final design. Fig. 6 also shows α as a function of s/d for different w values. Increasing w decreases α by reducing the current crowding in the center conductor.

Fig. 7 shows plots of $v_{\rm ph}$ versus frequency at $s/d = 0.3$. The dispersion in $v_{\rm ph}$ is minimal for $f > 5$ GHz, especially for the high h values. The decrease in $v_{\rm ph}$ for $f < 5$ GHz is reasonable because here R begins to approach and ultimately dominate the frequency dependent terms as discussed earlier.

Fig. 8 shows a typical Z_0 and α versus frequency behavior. For Z_0, there is no dispersion and its value is equal to 50 Ω. All this shows is that the Z_0 of this line is the same as the Z_0 of the through line used in the calibration standard. However, as discussed earlier regarding (3), above 10 GHz what is measured is quite accurate. In this range a frequency independent $v_{\rm ph}$ and Z_0 can be modeled using frequency independent L and C values in standard transmission theory. The loss data shows that α increases approximately with the square root of frequency due to skin depth penetration.

In the range of parameters used in the experiments several lines met the $v_{\rm ph}$ goal. But none of these lines also had a 50 Ω Z_0. Their Z_0 were in the range of 55 Ω–70 Ω. We now describe how a line meeting the design criteria can be realized. Fig. 9 shows Z_0 as a function of $h - b$ at $s/d = 0.3$ and $b = 9$ μm for different w values. Data for different w values fall on lines with approximately the same slope. This data and observation can be used to design for a specific Z_0 and $v_{\rm ph}$ as follows. As stated earlier, one can adjust w to achieve the desired Z_0 independent of $v_{\rm ph}$. Furthermore, it was shown in Fig. 4 that at $s/d = 0.3$, $h = 80$ μm slots give the desired $v_{\rm ph} = 8.9$ cm/nsec. A 50 Ω line with this phase velocity in Fig. 9 should have coordinates of $Z_0 = 50$ Ω and $h - b = 71$ μm. By plotting a line passing through this point with the same slope as the others we obtain another locus of data points corresponding to a different w value. A simple extrapolation yields a w value of 44 μm for this locus. Therefore a line with parameters $b = 9$ μm, $h = 80$ μm, $w = 44$ μm, and $s/d = 0.3$ should have $v_{\rm ph} = 8.9$ cm/nsec and $Z_0 = 50$ Ω. Using the data presented many other combinations of Z_0 and $v_{\rm ph}$ can be realized.

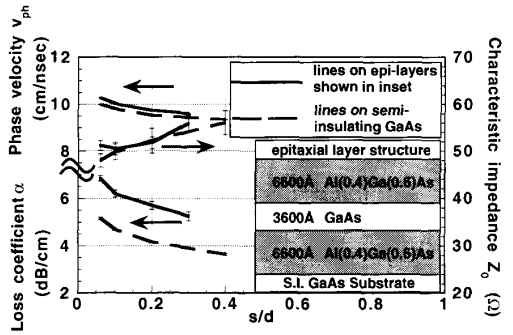

Fig. 10. Measured $v_{\rm ph}$, Z_0, and α for the (9,60,25) line on the MBE grown epitaxial layers superimposed with the results for the same line fabricated on semi-insulating GaAs.

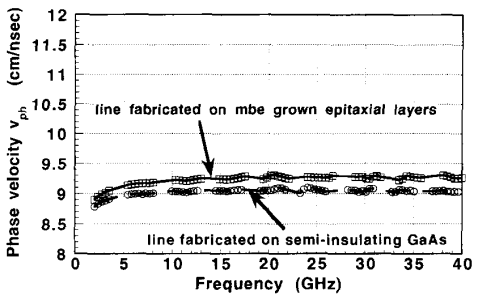

Fig. 11. Measured $v_{\rm ph}$ as a function of frequency on the MBE grown epitaxial layer for the (9,70,20) line at $s/d = 0.4$ superimposed with the results for the same line fabricated on semi-insulating GaAs.

VI. Results on Lines Fabricated on MBE Grown Epitaxial Layers

For device applications the slow wave electrodes would at least partially overlap with epitaxial layers. An epitaxial layer is essential to form the optical waveguide medium in a traveling wave electrooptic modulator. Therefore the behavior of slow wave transmission lines on epitaxial layers was investigated. The layer involved here were unintentionally doped and the background carrier concentration was believed to be p-type with a carrier concentration of less than 5×10^{14} cm^{-3}. Due to limited availability of this material only five different lines and two calibration standards were fabricated. The fabricated lines were subjected to the mechanical inspection previously outlined and found to be equivalent to the lines of the same dimensions fabricated on the semi-insulating wafer.

The epitaxial layer structure used in the experiments is shown in the inset of Fig. 10. It was grown by molecular beam epitaxy. This structure is intended to form a dielectric slab waveguide at optical frequencies. The layer thicknesses were confirmed under scanning electron microscope (SEM) examination and Al compositions by room temperature photoluminescence measurements.

Fig. 10 shows the results of these measurements superimposed on the results when the same line geometries were measured on semi-insulating material. The $v_{\rm ph}$ increased by about 2%, and there is no appreciable change in Z_0. No Z_0 change combined with a $v_{\rm ph}$ increase implies that L and C decreased together proportionally. The C decrease can be explained by the smaller dielectric constant of the AlGaAs material used in the epitaxial structure. The decrease in L may be explained by modeling the slots as series slotline stubs loading a uniform coplanar line. The decrease in $v_{\rm ph}$ due to the presence of AlGaAs material will decrease the electrical length of the slots. Therefore, the stub reactance, which is inductive, will be reduced. So a reduction in the inductance per unit length of the loaded line will result. A stub loaded coplanar line model developed with the tools described earlier gives results in very good agreement with the $v_{\rm ph}$ increase observed. Finally, Fig. 10 shows that α on these lines increased by 1.5 dB/cm compared to lines on semi-insulating GaAs. This is explained by the presence of mobile charge in the MBE layers due to unintentional background doping. This results in an increased conductivity for these layers which gives the observed loss increase.

Another concern with the transmission lines that are fabricated on epitaxial layers with mobile carriers is the possibility of $v_{\rm ph}$ dispersion due to conductivity variation of the material with frequency. Fig. 11 shows the variation of $v_{\rm ph}$ as a function of frequency for a particular line geometry fabricated on MBE grown epitaxial layers and semi-insulating GaAs substrates. As shown, $v_{\rm ph}$ increased uniformly over the measurement bandwidth and no anomalous dispersion effects were observed.

VII. Conclusions

In this work, a detailed experimental study of coplanar waveguide slow wave transmission lines was undertaken. In the study both semi-insulating GaAs substrates and MBE grown epitaxial layers on semi-insulating GaAs substrates were used. All the fabricated structures were very carefully examined and measured up to 40 GHz using coplanar microwave probes.

The slow wave structure consists of a coplanar transmission line with periodic slots cut into the ground conductors. It is shown that with this approach significant slowing of the phase velocity is possible. In the experiments a phase velocity value of 8.9 cm/nsec was achieved which represents a 22% slowing compared to the phase velocity of a uniform coplanar line.

It was found that the presence of the slots did not result in an increase of the loss coefficient. For a given slot depth almost all the phase velocity slowing is achieved when the slot width to slot period ratio is around 0.3. The periodic loading of the line due to the slots increases when the gaps between the center conductor and the ground planes are decreased. The width of the center conductor had no effect on the phase velocity although it did effect the characteristic impedance.

These observations suggested a way of using the measured data to tailor a slow wave structure for a specific phase velocity and characteristic impedance. First this requires choosing the gap of the unperturbed line for an acceptable loss. Then for a given gap the slot depth is adjusted until the desired phase velocity is achieved. It was found that the velocity slowing varies linearly as a function of slot depth for small slot depths for a slot width to period ratio of 0.3. Finally the center

conductor width is adjusted to get the desired characteristic impedance value. If more fine tuning is required one can vary the slot length to period ratio around the value of 0.3 chosen here. Dispersion in characteristic impedance and phase velocity is found to be minimal to 40 GHz both for devices on semi-insulating GaAs substrates and epitaxial layers.

REFERENCES

[1] R. C. Alferness, "Waveguide electrooptic modulators," *IEEE Trans. Microwave Theory Tech.*, vol. MTT-30, pp. 1121–1137, Aug. 1982.

[2] R. G. Walker, "High speed III-V electrooptic waveguide modulators," *IEEE J. Quantum Electron.*, vol. 27, pp. 654–667, Mar. 1991.

[3] S. Y. Wang and S. H. Lin, "High-speed III-V electrooptic waveguide modulators at $\lambda = 1.3$ μm," *J. Lightwave Tech.*, vol. 6, pp. 743–757, June 1988.

[4] W. H. Haydl, "Properties of meander coplanar transmission lines," *IEEE Microwave Guided Wave Lett.*, vol. 2, pp. 439–441, Nov. 1992.

[5] T. Wang and T. Itoh, "Confirmation of slow waves in a crosstie overlay coplanar waveguide and its applications to band-reject gratings and reflectors," *IEEE Trans. Microwave Theory Tech.*, vol. MTT-36, pp. 1811–1818, Dec. 1988.

[6] A. F. Harvey, "Periodic and guiding structures at microwave frequencies," *IRE Trans. Microwave Theory Tech.*, vol. MTT-8, pp. 30–61, Jan. 1960.

[7] N. A. F. Jaeger and Z. K. F. Lee, "Slow-wave electrode for use in compound semiconductor electrooptic modulators," *IEEE J. Quantum Electron.*, vol. 28, pp. 1778–1784, Aug. 1992.

[8] R. E. Collin, *Foundations for Microwave Engineering*. New York: McGraw-Hill, 1966, pp. 366–369.

[9] J. C. Yi, S. H. Kim, and S. S. Choi, "Finite-element method for the impedance analysis of traveling-wave modulators," *IEEE J. Lightwave Tech.*, vol. 8, pp. 817–822, Jun. 1990.

[10] HP Product Note 8510-8, Network Analysis—Applying the HP 8510B TRL Calibration for Non-Coaxial Measurements, Oct. 1987.

[11] G. L. Matthaei, G. C. Chinn, C. H. Plott, and N. Dagli, "A simplified means for computation of interconnect distributed capacitances and inductances," *IEEE Trans. Computer Aided Design*, vol. 11, pp. 513–523, Apr. 1992.

[12] EESOF corporation, *Linecalc*, transmission line analysis and synthesis program, version 3.5.

[13] K. Kiziloglu, N. Dagli, G. L. Matthaei, and S. I. Long, "Experimental analysis of transmission line parameters in high-speed GaAs digital circuit interconnects," *IEEE Trans. Microwave Theory Tech.*, vol. 39, pp. 1361–1366, Aug. 1991.

[14] R. K. Hoffman, *Handbook of Microwave Integrated Circuits*. Norwood, MA: Artech House, 1987, pp. 355.

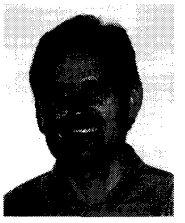

Ralph Spickermann was born March 3, 1965 in Santa Clara, CA. He received the B.S. degree in electrical engineering and computer science from the University of California at Berkeleyand the M.S. degree in electrical engineering from the University of California at Santa Barbara in 1986 and 1991, respectively. He is currently pursuing the Ph.D. degree at the latter university.

From 1986 to 1989, he was employed at Teledyne MEC in Palo Alto, CA where he worked on the design and production of traveling wave tubes for radar and satellite communications applications.

Nadir Dagli (S'77–M'86) was born in Ankara, Turkey. He received the B.S. and M.S. degrees in electrical engineering from Middle East Technical University, Ankara, Turkey in 1976 and 1979, respectively, and the Ph.D. degree, also in electrical engineering, from Massachusetts Institute of Technology, Cambridge, in 1986.

After graduation, he joined the electrical and computer engineering department at University of California at Santa Barbara, where he is currently an Associate Professor. His current interests are design, fabrication, and modeling of guided-wave components for optical integrated circuits, solid-state microwave and millimeter-wave devices, calculations on the optical properties of quantum wires, electron waveguides, and novel quantum interference devices based on electron waveguides.

Dr. Dagli was awarded NATO science and IBM predoctoral fellowships during his graduate studies. He is the recipient of 1990 UCSB Alumni Distinguished Teaching Award and 1990 UC Regents Junior Faculty Fellowship.